

# Surface Acidity and Properties of TiO<sub>2</sub>/SiO<sub>2</sub> Catalysts Prepared by Atomic Layer Deposition: UV–visible Diffuse Reflectance, DRIFTS, and Visible Raman Spectroscopy Studies

Junling Lu,<sup>†</sup> Kathryn M. Kosuda,<sup>†</sup> Richard P. Van Duyne,<sup>†</sup> and Peter C. Stair<sup>†,‡,\*</sup>

Department of Chemistry and Center for Catalysis and Surface Science, Northwestern University, Evanston, Illinois 60208, and Chemical Sciences and Engineering Division, Argonne National Laboratory, Argonne, Illinois 60439

Received: March 11, 2009; Revised Manuscript Received: May 1, 2009

Highly uniform submonolayer to multilayer thin films of titanium dioxide supported on high surface area silica gel have been synthesized by atomic layer deposition (ALD) using titanium tetrachloride (TiCl<sub>4</sub>) and titanium isopropoxide (TTIP) as metal precursors. The deposition rate of titania films from TiCl<sub>4</sub> was found to be stable in the 150–300 °C temperature range, which is slightly higher than that from TTIP at 150 °C. UV–visible diffuse reflectance spectroscopy (DRS) shows that the coordination geometry of Ti cations depends on the number of ALD cycles and the precursor but is essentially independent of deposition temperature. Using diffuse reflectance infrared Fourier transform spectroscopy (DRIFTS) and visible Raman spectroscopy with pyridine as a probe molecule, we found all of the titania films studied to exhibit Lewis acidity but only films containing chloride or carbonyl impurities possessed Brønsted acid sites. Additionally, three new pronounced bands in the Raman spectra,  $\nu_{6b}$  (638 cm<sup>-1</sup>),  $\nu_{9a}$  (1200 cm<sup>-1</sup>), and  $\nu_2$  (3103 cm<sup>-1</sup>), provide strong spectroscopic evidence for Brønsted acid sites on the surface.

## 1. Introduction

TiO<sub>2</sub>/SiO<sub>2</sub>-supported oxides have attracted considerable attention not only as advanced materials and catalytic supports but also as catalysts themselves<sup>1</sup> such as for isomerization of olefins,<sup>2</sup> epoxidation of olefins with H<sub>2</sub>O<sub>2</sub>,<sup>3</sup> dehydration,<sup>4–7</sup> and selective oxidation.<sup>8</sup> They have been considered as substitutes for pure TiO<sub>2</sub> because of their improved mechanical strength, thermal stability, and high dispersion of TiO<sub>2</sub>.<sup>9–11</sup> The catalytic properties of dispersed titania species have been found to be strongly dependent on their local structures. Gao et al.<sup>12</sup> showed that highly dispersed surface titania species exhibit completely different catalytic behavior for methanol oxidation compared to bulk titania; redox products form preferentially on the dispersed titania species, while dehydration products form primarily on bulk titania. Bonelli et al.<sup>13</sup> also found isolated Ti<sup>4+</sup> cations of TiO<sub>2</sub>/SiO<sub>2</sub> catalysts have stronger Lewis acidity for catalyzing the transesterification of refined oil with methanol.

Although significant progress has been made in understanding the physical and chemical properties of silica-supported titania, the nature of their acidity is still debated as highlighted by Notari et al. in 2006.<sup>14</sup> Briefly, their work provided strong evidence that high purity TiO<sub>2</sub>/SiO<sub>2</sub>-mixed oxides do not have Brønsted acid sites, which is in conflict with previous studies in the 1990s by Tanabe,<sup>15</sup> Ko,<sup>16</sup> Liu,<sup>17</sup> and Doolin.<sup>18</sup> This discrepancy with previous results was very likely due to, in some instances, the presence of acid-inducing impurities in materials used in earlier work and in other instances to the methods used to detect Brønsted acidity. Very recently, the opposite conclusions were also obtained for TiO<sub>2</sub>/SiO<sub>2</sub>-supported oxides. Bonelli et al.<sup>13</sup> found Brønsted acid sites on TiO<sub>2</sub>/SiO<sub>2</sub>-supported oxides with

high TiO<sub>2</sub> loading (>8 wt %) by means of Fourier transform infrared (FTIR) measurements of CO and NH<sub>3</sub> adsorption. However, Gao et al. reported TiO<sub>2</sub>-grafted silica MCM-41 catalysts contain only Lewis acid sites on the surface, where the grafted TiO<sub>2</sub> were in a highly dispersed amorphous form.<sup>19</sup>

Atomic layer deposition (ALD) is a thin film growth technique, which relies on self-limiting binary reactions between gaseous precursor molecules and a substrate to deposit films in a layer-by-layer fashion. The deposited amount can be precisely controlled simply by adjusting the number of deposition cycles. Since the development of the technique in the late 1970s by Suntola et al.,<sup>20</sup> ALD has been widely used in research laboratories and industry to grow thin-film electroluminescent devices,<sup>21</sup> high-*k* dielectric gate materials,<sup>22</sup> and wear-resistant coatings.<sup>23</sup> Considerable research has been undertaken to better understand the chemistry and extend the range of materials that can be deposited. Very recently, a few groups have expanded its application to synthesize catalytic materials,<sup>24–26</sup> and the merits of the method for the synthesis of next generation catalysts have been discussed.<sup>27,28</sup>

TiO<sub>2</sub> films grown by ALD are one of the most explored systems where titanium tetrachloride (TiCl<sub>4</sub>) and titanium isopropoxide (TTIP) are widely used as metal precursors and water or hydrogen peroxide are used as oxygen precursors.<sup>29–36</sup> Considerable work has been performed to study the growth mechanism on flat surfaces using a quartz crystal microbalance (QCM)<sup>32</sup> and in situ infrared (IR) spectroscopy.<sup>33</sup> Only a few studies have been performed on high surface area powders.<sup>34–36</sup> Using TTIP as the metal precursor followed by oxidation, Keränen et al.<sup>36</sup> reported a growth rate of 1 Ti atom/nm<sup>2</sup> per ALD cycle over the relatively narrow temperature range of 110–180 °C, while titania can be grown over a much wider temperature range from 80 to 600 °C using TiCl<sub>4</sub> as the precursor.<sup>30</sup>

\* To whom correspondence should be addressed. E-mail: pstair@northwestern.edu.

<sup>†</sup> Northwestern University.

<sup>‡</sup> Argonne National Laboratory.

# Report Documentation Page

Form Approved  
OMB No. 0704-0188

Public reporting burden for the collection of information is estimated to average 1 hour per response, including the time for reviewing instructions, searching existing data sources, gathering and maintaining the data needed, and completing and reviewing the collection of information. Send comments regarding this burden estimate or any other aspect of this collection of information, including suggestions for reducing this burden, to Washington Headquarters Services, Directorate for Information Operations and Reports, 1215 Jefferson Davis Highway, Suite 1204, Arlington VA 22202-4302. Respondents should be aware that notwithstanding any other provision of law, no person shall be subject to a penalty for failing to comply with a collection of information if it does not display a currently valid OMB control number.

1. REPORT DATE <b>JUN 2009</b>		2. REPORT TYPE		3. DATES COVERED <b>00-00-2009 to 00-00-2009</b>	
4. TITLE AND SUBTITLE <b>Surface Acidity and Properties of TiO<sub>2</sub>/SiO<sub>2</sub> Catalysts Prepared by Atomic Layer Deposition: UV-visible Diffuse Reflectance, DRIFTS, and Visible Raman Spectroscopy Studies</b>				5a. CONTRACT NUMBER	
				5b. GRANT NUMBER	
				5c. PROGRAM ELEMENT NUMBER	
6. AUTHOR(S)				5d. PROJECT NUMBER	
				5e. TASK NUMBER	
				5f. WORK UNIT NUMBER	
7. PERFORMING ORGANIZATION NAME(S) AND ADDRESS(ES) <b>Northwestern University, Department of Chemistry, 2145 Sheridan Road, Evanston, IL, 60208</b>				8. PERFORMING ORGANIZATION REPORT NUMBER	
9. SPONSORING/MONITORING AGENCY NAME(S) AND ADDRESS(ES)				10. SPONSOR/MONITOR'S ACRONYM(S)	
				11. SPONSOR/MONITOR'S REPORT NUMBER(S)	
12. DISTRIBUTION/AVAILABILITY STATEMENT <b>Approved for public release; distribution unlimited</b>					
13. SUPPLEMENTARY NOTES					
14. ABSTRACT					
15. SUBJECT TERMS					
16. SECURITY CLASSIFICATION OF:			17. LIMITATION OF ABSTRACT <b>Same as Report (SAR)</b>	18. NUMBER OF PAGES <b>7</b>	19a. NAME OF RESPONSIBLE PERSON
a. REPORT <b>unclassified</b>	b. ABSTRACT <b>unclassified</b>	c. THIS PAGE <b>unclassified</b>			

In the current study, we used TiCl<sub>4</sub> and TTIP as metal precursors and water as the oxygen precursor to synthesize TiO<sub>2</sub>/SiO<sub>2</sub> materials. The amount of ALD TiO<sub>2</sub> deposited on silica gel was determined by inductively coupled plasma atomic emission spectroscopy (ICP-AES). The coordination geometry of Ti cations in the films was characterized by UV–visible diffuse reflectance spectroscopy (UV–vis DRS). Furthermore, the acidity of TiO<sub>2</sub>/SiO<sub>2</sub> catalysts prepared by ALD was investigated by combined diffuse reflectance infrared Fourier transform spectroscopy (DRIFTS) and visible (488 nm) Raman spectroscopy, where the potential for probing Brønsted acid sites with Raman spectroscopy was explored.

## 2. Experimental Section

**2.1. Sample Preparation.** Silicycle S10040M SiO<sub>2</sub> with a surface area of ~100 m<sup>2</sup>/g, a primary particle size of 75–200 μm, and a nominal pore diameter of 30 nm was used as the support. TiO<sub>2</sub> ALD was performed using a viscous flow reactor described previously.<sup>37,38</sup> The high surface area silica gel powder was loaded into a fixed bed powder holder, which consists of a tray constructed from 304 stainless steel with dimensions of 143 mm × 29 mm × 3.2 mm and a mesh stainless steel wire cloth cover (200 × 600, per linear inch) supported by a perforated stainless steel plate. The fine mesh cover prevents convective gas currents from disturbing the flat powder layer at the bottom of the powder tray, while allowing efficient diffusion of reactant and product gases in and out of the powder bed. For each ALD sample, ~1.0 g of silica gel was homogeneously spread into the powder tray.<sup>38</sup>

The TiO<sub>2</sub> films were deposited at temperatures of 150–300 °C using alternating exposure to titanium tetrachloride (TiCl<sub>4</sub>, Sigma-Aldrich, 99%) and Millipore water with a dose time of 50 s and a purge time of 150 s, where the TiCl<sub>4</sub> and water reservoirs were both kept at room temperature. The dose time necessary to achieve saturation coverage was determined using direct weight gain measurements by an analytical microbalance and by X-ray fluorescence (XRF). When the titanium isopropoxide (TTIP, Sigma-Aldrich, 97%) metal precursor was used, the TTIP reservoir was heated to 100 °C to achieve sufficient vapor pressure and reasonable dose times.<sup>36</sup> The inlet lines were also heated to 140 °C to prevent TTIP condensation on the inner wall of the inlet lines. The TiO<sub>2</sub> films prepared with TTIP were deposited at 150 °C with a TTIP dose time of 60 s, a water dose time of 120 s, and a purge time of 240 s. For both precursors, ultrahigh purity (99.999%) nitrogen was used as a carrier gas at a flow rate of 360 sccm and a pressure of ~1.3 Torr.

The amounts of ALD TiO<sub>2</sub> deposited on silica gel were determined by ICP-AES, and the quantity of chlorine impurities in the TiO<sub>2</sub>/SiO<sub>2</sub> prepared from TiCl<sub>4</sub> was determined by XRF. The surface area was obtained by low-temperature nitrogen adsorption using a Micromeritics ASAP 2010 apparatus, and the pore diameter was determined using the BJH desorption method.<sup>39</sup>

**2.2. UV–Vis DRS Measurements.** DR spectra were recorded under ambient conditions on a Varian Cary 1E UV–vis spectrophotometer equipped with a diffuse reflectance attachment (Keck facility at Northwestern University), using MgO as the reference. The TiO<sub>2</sub>/SiO<sub>2</sub> samples were loaded into a powder holder with a UV window to be sure that the sample thickness was greater than 1 mm. For comparison, commercial anatase titania was also measured. The edge energy ( $E_g$ ) for allowed transitions was determined by finding the intercept of the straight line in the low energy rise of a plot of  $[F(R_\infty)]^2/h\nu$  against the photon energy,  $h\nu$ .<sup>12</sup>

**2.3. DRIFTS Measurements.** All DRIFTS measurements were performed at room temperature using a Thermo Nicolet Nexus 870 instrument with an MCT detector (KECKII at Northwestern University). Each spectrum was collected using 256 scans with a resolution of 4 cm<sup>-1</sup>. Pyridine (EMD Chemicals, 99.0%) was carried to the sample by ultrahigh purity (99.999%) nitrogen flowing over a pyridine reservoir. Before pyridine adsorption, the TiO<sub>2</sub>/SiO<sub>2</sub> samples were purged for 30 min. After saturation, the TiO<sub>2</sub>/SiO<sub>2</sub> samples were purged for another 30 min to remove weakly bound, physisorbed pyridine.

**2.4. Raman Measurements.** The Raman spectra of 100 mg TiO<sub>2</sub>/SiO<sub>2</sub> samples in a fluidized bed reactor at atmosphere<sup>40</sup> were collected using 488 nm excitation at room temperature. Before pyridine adsorption, the TiO<sub>2</sub>/SiO<sub>2</sub> samples were purged with helium for 30 min, and then 100 μL pyridine was injected with a syringe and carried by helium to the catalyst bed. After saturation, the TiO<sub>2</sub>/SiO<sub>2</sub> samples were purged for another 30 min to remove weakly bound, physisorbed pyridine. The Raman shift was calibrated with cyclohexane and 4-acetamidophenol standards.

## 3. Results

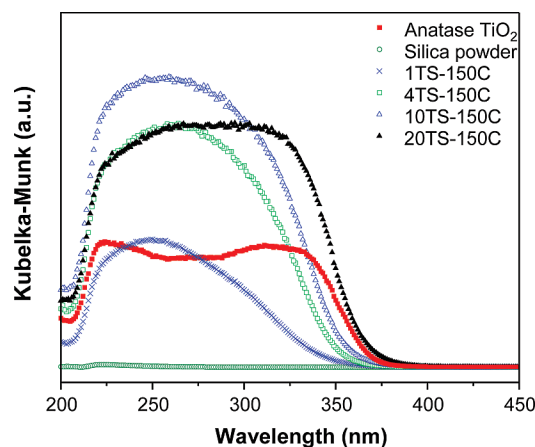
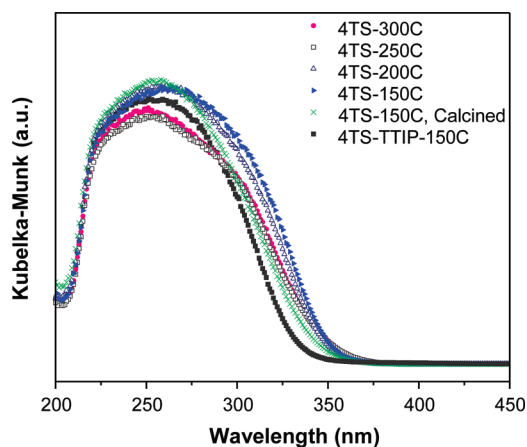
**3.1. TiO<sub>2</sub> ALD on Silica Gel.** Table 1 shows the physical and chemical properties of as-prepared TiO<sub>2</sub>/SiO<sub>2</sub> samples prepared with TiCl<sub>4</sub> at different temperatures and TTIP at 150 °C. For all cases, the amount of titania deposited in the first cycle was higher than for subsequent cycles. Between 1 and 10 cycles, the surface area exhibited only minor changes, while the average pore diameter increased after the first deposition cycle and then slightly decreased with subsequent cycles. When TiCl<sub>4</sub> was used as the metal precursor, chlorine impurities were detectable by XRF on the as-prepared samples. The amount of chlorine increased with the number of deposition cycles and with decreasing deposition temperature. For example, the weight percentage of chlorine impurities was about 0.48%, 0.9%, and 1.35% after 4 cycles of TiO<sub>2</sub> grown at 300 °C (4TS-300C), 4 cycles grown at 150 °C (4TS-150C), and 10 cycles grown at 150 °C (10TS-150C), respectively. However, chlorine impurities could be completely removed from the surface by either calcination in air at 500 °C for 2 h or by wet nitrogen purging for 24 h in the chamber at the deposition temperature (wet nitrogen consists of ~2% water in high purity nitrogen).<sup>41</sup> After either of these treatments, the amount of chlorine was below the XRF detection limit.

The growth rate of TiO<sub>2</sub> averaged over the first 10 cycles was almost constant between 150 and 300 °C, varying from 1.1 to 1.0 titanium atoms/nm<sup>2</sup> per cycle with TiCl<sub>4</sub> as the metal precursor. The growth rate was lower, 0.8 titanium atoms/nm<sup>2</sup> per cycle, for the TTIP precursor at 150 °C, which is slightly lower than the value reported by Keränen et al.<sup>36</sup> The lower growth rate using TTIP compared to that of TiCl<sub>4</sub> is attributed to a steric effect caused by the difference in size between the ligands of the two precursors.

**3.2. UV–Vis DRS.** The DR spectra from a series of as-prepared TiO<sub>2</sub>/SiO<sub>2</sub> samples grown at 150 °C ( $x$ TS-150C, where  $x$  is the number of cycles (1, 4, 10, and 20)) are depicted in Figure 1, where silica gel and anatase titania were also measured for comparison. As expected, pure silica gel has almost no absorption to 200 nm. 1TS-150C samples showed a broad band centered at approximately 250 nm, indicating the presence of isolated tetrahedrally coordinated Ti cations.<sup>1,12,36,52</sup> With an increasing number of cycles, the transition band became broader and increased in intensity, which signifies the formation of Ti cations having 5-fold and 6-fold coordination

**TABLE 1: Physical and Chemical Properties of As-Prepared TiO<sub>2</sub>/SiO<sub>2</sub> ALD Samples from the TiCl<sub>4</sub> or TTIP Precursor**

ALD samples	titania (wt %)	titanium (atoms/nm <sup>2</sup> )	BET surface area (m <sup>2</sup> /g)	pore diameter (Å)	chlorine (wt %, XRF)	<i>E<sub>g</sub></i> (eV)
silica powder			91.6	301.5		
anatase TiO <sub>2</sub>						3.47
1TS-TTIP-150C	1.92	1.58	96.0	312.6	— <sup>a</sup>	4.16
4TS-TTIP-150C	4.86	4.00	100.8	306.2	—	3.90
7TS-TTIP-150C	7.68	6.32	—	—	—	3.83
10TS-TTIP-150C	9.98	8.21	101.8	294.0	—	3.78
1TS-150C	2.34	1.92	90.9	329.1	0.53	3.87
4TS-150C	6.31	5.19	93.8	306.1	0.90	3.68
7TS-150C	10.31	8.48	—	—	—	3.73
10TS-150C	13.48	11.10	92.8	312.1	1.35	3.61
20TS-150C	24.31	20.01	—	—	1.72	3.50
1TS-200C	1.75	1.44	94.7	312.1	—	3.84
4TS-200C	6.07	5.00	94.0	309.0	0.80	3.71
7TS-200C	9.49	7.81	—	—	—	3.65
10TS-200C	12.85	10.57	94.1	296.8	—	3.61
1TS-250C	2.30	1.90	93.4	325.5	—	3.82
4TS-250C	5.89	4.85	94.7	323.9	0.65	3.76
7TS-250C	9.49	7.82	—	—	—	3.65
10TS-250C	12.88	10.60	95.5	306.0	—	3.65
1TS-300C	2.20	1.81	94.8	320.0	—	3.94
4TS-300C	5.57	4.59	103.7	303.0	0.48	3.71
7TS-300C	8.92	7.36	—	—	—	3.65
10TS-300C	12.43	10.22	89.7	308.4	—	3.64

<sup>a</sup> Not measured.**Figure 1.** UV-vis DR spectra of silica powder, anatase TiO<sub>2</sub>, and as-prepared TiO<sub>2</sub>/SiO<sub>2</sub> ALD samples deposited at 150 °C from TiCl<sub>4</sub> under ambient conditions.**Figure 2.** UV-vis DR spectra of 4-cycle TiO<sub>2</sub>/SiO<sub>2</sub> ALD samples under ambient conditions.

numbers.<sup>12,36,52</sup> Figure 2 compares 4-cycle ALD samples from TiCl<sub>4</sub> and TTIP (4TS-TTIP-150C) prepared at different temperatures. The transition band intensity from the 4TS-TTIP-150C sample was lower than the 4-cycle samples prepared with TiCl<sub>4</sub> due to the lower growth rate with this precursor. The observed edge energies, *E<sub>g</sub>*, reported in Table 1 were also generally consistent with titania loading. The 4TS-150C sample calcined at 500 °C showed a blue shift (*E<sub>g</sub>* = 3.87 eV), which is most likely due to partial dehydration.<sup>12</sup>

**3.3. DRIFTS.** Figure 3 shows the DRIFT spectra obtained from pyridine adsorption on the as-prepared *x*TS-150C samples from TiCl<sub>4</sub>. Two pronounced peaks at 1538 and 1637 cm<sup>-1</sup>, whose intensity increased with the number of titania deposition cycles, indicate the presence of Brønsted acid sites on these TiO<sub>2</sub>/SiO<sub>2</sub> samples.<sup>18,42,43</sup> In the OH stretch region, one sharp negative peak at 3745 cm<sup>-1</sup> is assigned to silanol groups, and a less pronounced, broad negative peak at 3680 cm<sup>-1</sup> (denoted by \*) is assigned to Ti-OH groups. After pyridine adsorption, the OH stretch shifted to 2520 cm<sup>-1</sup> for the TiO<sub>2</sub>/SiO<sub>2</sub> samples with more than one cycle (~2780 cm<sup>-1</sup> for pure silica gel and

~2570 cm<sup>-1</sup> for 1TS-150C). These features are assigned to the interaction of isolated silanols and Ti-OH species with pyridine molecules via the formation of hydrogen bonds. Obviously, more acidic hydroxyl groups were present on the as-prepared TiO<sub>2</sub>/SiO<sub>2</sub> samples because the shift was significantly stronger for pyridine on as-prepared *x*TS-150C samples than that on pure silica gel. The silica gel surface was gradually covered by TiO<sub>2</sub> with increasing numbers of deposition cycles as indicated by the consumption of silanol groups. However, the silica surface was not completely covered even after 20 cycles (~3.6 ML, 1 ML ≈ 5.5 Ti atoms/nm<sup>2</sup>)<sup>44</sup> because isolated silanol groups were still perturbed by pyridine as evidenced by the negative peak at 3745 cm<sup>-1</sup> in the DRIFT spectra (Figure 3a).

Figure 4 shows pyridine adsorption on 4-cycle TiO<sub>2</sub>/SiO<sub>2</sub> samples prepared with TiCl<sub>4</sub> and TTIP. Again, the bands at 1538 and 1637 cm<sup>-1</sup> assigned to a pyridinium ion were present on all of the as-prepared 4-cycle samples prepared from TiCl<sub>4</sub> at different temperatures (Figure 4a-d). However, these bands diminished to the noise level once chlorine was removed using a wet N<sub>2</sub> purge (Figure 4e) or calcination in air at 500 °C (Figure 4f). The OH stretching band observed upon adsorption of

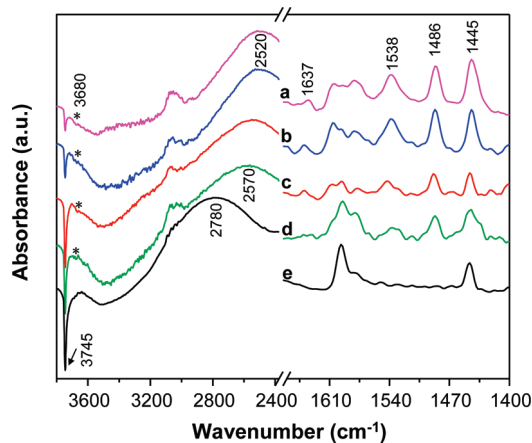


**Figure 3.** DRIFT spectra of pyridine adsorption on silica powder and as-prepared TiO<sub>2</sub>/SiO<sub>2</sub> ALD samples deposited at 150 °C from TiCl<sub>4</sub>: (a) 20TS-150C, (b) 10TS-150C, (c) 4TS-150C, (d) 1TS-150C, and (e) SiO<sub>2</sub>.

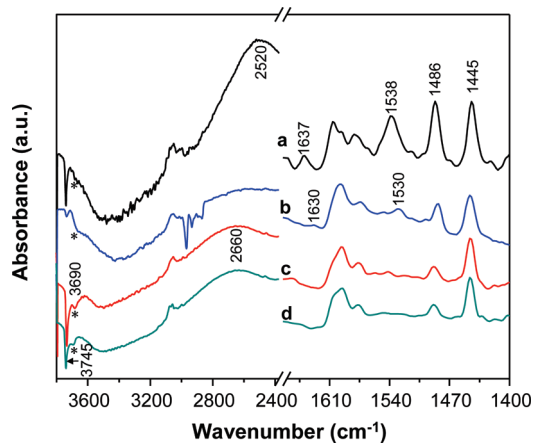


**Figure 5.** DRIFT spectra of pyridine adsorption on 10-cycle TiO<sub>2</sub>/SiO<sub>2</sub> ALD samples: (a) 10TS-150C, (b) 10TS-TTIP-150C, (c) 10TS-150C, wet N<sub>2</sub>-purged, and (d) 10TS-TTIP-150C, calcined at 500 °C in oxygen for 2 h.

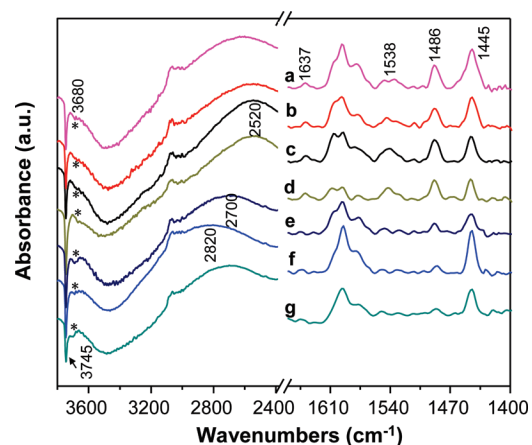


**Figure 4.** DRIFT spectra of pyridine adsorption on 4-cycle TiO<sub>2</sub>/SiO<sub>2</sub> ALD samples: (a) 4TS-300C, (b) 4TS-250C, (c) 4TS-200C, (d) 4TS-150C, (e) 4TS-150C, wet N<sub>2</sub>-purged, (f) 4TS-150C, calcined in air at 500 °C for 2 h, and (g) 4TS-TTIP-150C, calcined at 500 °C in oxygen for 2 h.

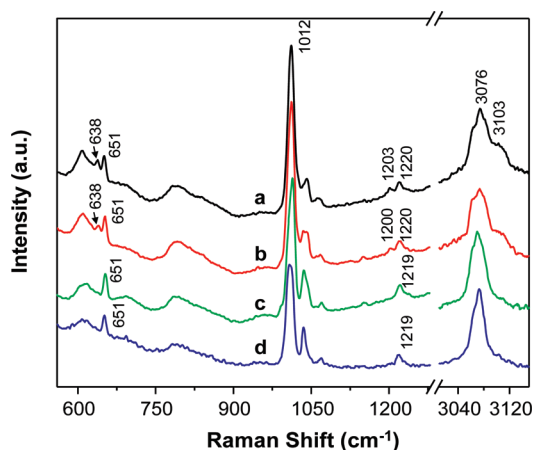


**Figure 6.** Visible Raman spectra of pyridine adsorption on 4-cycle TiO<sub>2</sub>/SiO<sub>2</sub> ALD samples from TiCl<sub>4</sub>: (a) 4TS-150C, (b) 4TS-200C, (c) 4TS-150C, wet N<sub>2</sub>-purged, and (d) 4TS-150C, calcined in air at 500 °C for 2 h.

pyridine was found at 2700 cm<sup>-1</sup> for the wet N<sub>2</sub>-purged sample and 2820 cm<sup>-1</sup> for the calcined sample, close to the OH frequency of 2780 cm<sup>-1</sup> on pure silica gel. The 4-cycle TiO<sub>2</sub>/SiO<sub>2</sub> sample from TTIP (4TS-TTIP-150C), calcined for two hours at 500 °C in oxygen, showed the same features as the 4-cycle wet N<sub>2</sub>-purged and calcined samples from TiCl<sub>4</sub>, i.e., no Brønsted acid sites were present on the surface.

In order to better understand the dependence of acidity on the loading of titania, pyridine adsorption on different 10-cycle TiO<sub>2</sub>/SiO<sub>2</sub> samples was also performed and is shown in Figure 5. Pyridine adsorption on the 10TS-150C sample after wet N<sub>2</sub> purging did not show bands due to pyridinium ions at 1538 and 1637 cm<sup>-1</sup> (Figure 5c). The as-prepared 10TS-TTIP-150C sample (Figure 5b) showed relatively fewer and weaker Brønsted acid sites at 1530 and 1630 cm<sup>-1</sup> compared with those of the as-prepared 10TS-150C sample from TiCl<sub>4</sub> (Figure 5a). However, the as-prepared TiO<sub>2</sub>/SiO<sub>2</sub> samples from TTIP contained some amount of carbonyl, indicated by the negative peaks between 2800 and 3000 cm<sup>-1</sup> in spectrum b of Figure 5. Carbonyl is produced by incomplete removal of isopropanol ligands from TTIP. However, the bands at 1538 and 1637 cm<sup>-1</sup> due to pyridinium ions disappeared together with the carbonyl bands after calcination at 500 °C in oxygen (Figure 5d). These results indicate that the Brønsted acid sites on all of TiO<sub>2</sub>/SiO<sub>2</sub>

samples are related to chlorine or carbonyl impurities and not to the intrinsic Ti–O–Si interface.

**3.4. Raman Spectroscopy.** Compared with IR spectroscopy,<sup>13,14,17–19,42,43</sup> Raman spectroscopy has rarely been applied to study the acidity of catalysts using pyridine as a probe molecule.<sup>45–49</sup> Raman spectroscopy is sensitive to adsorption on Lewis acid sites and to species adsorbed by H-bond interactions, but bands characteristic of adsorption on Brønsted acid sites have been difficult to identify.<sup>46,47</sup> Sample fluorescence is also often a problem. To the best of our knowledge, Hendra was the first to apply Raman spectroscopy in studies of surface acidity using adsorbed pyridine on oxide surfaces.<sup>45,46</sup> Here, we demonstrate the application of Raman spectroscopy to further explore the Brønsted acid sites of TiO<sub>2</sub>/SiO<sub>2</sub> samples prepared with ALD.

As shown in Figure 6, in the range of Raman shifts where the two ring-breathing modes of pyridine appear (990 to 1050 cm<sup>-1</sup>), all of the 4-cycle samples exhibited two very similar peaks at 1013 and 1042 cm<sup>-1</sup> corresponding to  $\nu_1$  and  $\nu_{12}$  ring-breathing modes, respectively. An examination of the spectra from the various samples indicates that these modes are relatively insensitive to the presence of Brønsted acid sites<sup>46</sup> compared with the DRIFT spectra (Figure 4c–f). This is due to the strong overlap between the ring-breathing bands from H-bonded pyridine species (HPy) and pyridinium ions (BPy).

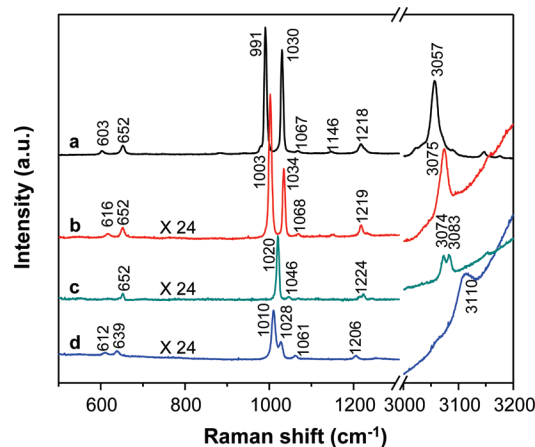


**Figure 7.** Visible Raman spectra of pyridine in different solutions: (a) neat pyridine, (b) aqueous pyridine (0.5 mol/L), (c) aqueous pyridine (0.5 mol/L) + ZnCl<sub>2</sub> (~1 ML), and (d) aqueous pyridine (0.5 mol/L) + HCl (1 mol/L).

However, two distinct peaks around 638 cm<sup>-1</sup> and 1200 cm<sup>-1</sup> together with a broad shoulder at ~3103 cm<sup>-1</sup> in the C–H stretch range were observed on the as-prepared 4-cycle samples prepared with TiCl<sub>4</sub> (Figure 6a,b) where Brønsted sites were present but were not observed on the wet N<sub>2</sub>-purged (Figure 6c) or calcined (Figure 6d) 4TS-150C samples. Therefore, these vibrational modes can be used to provide information on BPY.

To confirm the assignment of these peaks, the spectra of neat pyridine, aqueous pyridine (0.5 mol/L), aqueous pyridine (0.5 mol/L) + HCl (1 mol/L), and aqueous pyridine (0.5 mol/L) + ZnCl<sub>2</sub> complex (1 mol/L) were measured. The results are shown in Figure 7. Aqueous pyridine has peaks at 3075, 1219, 1068, 1034, 1003, 652, and 616 cm<sup>-1</sup>. They are assigned to the bands of H-bonded pyridine (HPy). Pyridine + HCl shows peaks at 3110, 1206, 1061, 1028, 1010, 639, and 612 cm<sup>-1</sup>, which are assigned to the pyridinium ions and correspond to the bands of species adsorbed on the Brønsted acid sites (BPY). Pyridine + ZnCl<sub>2</sub> shows peaks at 3083, 3074, 1224, 1046, 1020, and 652 cm<sup>-1</sup>, corresponding to bands of species adsorbed on Lewis acid sites (LPy). Therefore, the two extra peaks at 638 cm<sup>-1</sup> and 1200 cm<sup>-1</sup> ( $\nu_{6b}$  and  $\nu_{9a}$  C–H bending modes, respectively) found on the as-prepared 4-cycle samples prepared with TiCl<sub>4</sub> (Figure 6a,b) can be assigned to pyridinium ions.<sup>49,50</sup>

## 4. Discussion

**4.1. Structure of Supported Titania ALD Films.** An understanding of the coordination geometry of Ti cations, especially at the Ti–O–Si interface, is of importance for establishing the relationships between structure, acidity, and catalytic properties. The present study helps to clarify whether Brønsted acid sites can be created by a charge imbalance at the Ti–O–Si interface as proposed by Tanabe.<sup>15</sup>

UV–vis DR spectra are usually employed to provide information about the coordination geometry of Ti cations (first coordination sphere) and changes in the ligands (second coordination sphere).<sup>1,12</sup> For amorphous or crystalline TiO<sub>2</sub>/SiO<sub>2</sub>-mixed oxides and for TiO<sub>2</sub>/SiO<sub>2</sub>-supported oxides synthesized by various methods such as incipient wetness impregnation, liquid phase grafting, and chemical vapor deposition (CVD), the absorption band always shows the same trend. At low Ti concentration, the Ti cations are 4-fold coordinated, and the coordination number increases to 5-fold and 6-fold with increasing Ti loading.<sup>1,12,51,52</sup>

TiO<sub>2</sub>/SiO<sub>2</sub> ALD samples showed the same trend in the UV–vis DR spectra as samples prepared by other methods. In the case of the 1TS-150C sample, the broad ligand to metal charge transfer (LMCT) transition band centered at about 250 nm can be decomposed into at least three peaks around 223, 241, and 285 nm (individual curves are not shown here). The transition band shoulder around 223 nm is characteristic of isolated Ti cations in symmetric tetrahedral sites.<sup>1,12,52</sup> The main band at ~241 nm can be assigned to isolated tetrahedrally coordinated Ti cations in low symmetry environments such as on the pore surface where one or more ligands are water or OH groups.<sup>52</sup> The broad shoulder at 285 nm is assigned to partially condensed Ti–O–Ti species such as 5-fold coordinated Ti cations.<sup>52</sup> For the 4TS-150C sample, the transition band around 285 nm becomes dominant with an additional weak shoulder near 325 nm, which signifies the formation of 6-fold coordinated Ti cations.<sup>12,52</sup> With further deposition of TiO<sub>2</sub> to 10 and 20 ALD cycles, the transition band near 325 nm grows quickly, consistent with the predominant formation of six-coordinate Ti cations at higher titania loading.

For the corresponding band gap edge energy, Gao et al.<sup>12</sup> reported that surface Ti cations in a 1% TiO<sub>2</sub>/SiO<sub>2</sub> (0.24 Ti atoms/nm<sup>2</sup>) supported oxide are predominately isolated TiO<sub>4</sub> units with an edge energy at 4.66 eV, whereas at approximately monolayer coverage, (~4 Ti atoms/nm<sup>2</sup>) two-dimensional, polymerized TiO<sub>5</sub> species are found with an edge energy at 3.78 eV. The titania loading and edge energy of TiO<sub>2</sub>/SiO<sub>2</sub> ALD samples are shown in Table 1. The 1TS-150C sample (1.92 Ti atoms/nm<sup>2</sup>) contains predominately four-coordinate and five-coordinate Ti cations with an edge energy of 3.87 eV. Ti cations in the 4TS-150C sample (5.19 Ti atoms/nm<sup>2</sup>,  $E_g = 3.68$  eV) are assigned as six-coordinate under hydrated conditions or five-coordinate under dehydrated conditions. The 10TS-150C sample (11.1 Ti atoms/nm<sup>2</sup>,  $E_g = 3.61$  eV) contains mainly six-coordinate Ti cations under dehydrated conditions. The edge energy of the titania films from TiCl<sub>4</sub> is essentially independent of deposition temperature. Additionally, the titania films from TTIP show higher edge energies than those from TiCl<sub>4</sub>. For example, the 10TS-TTIP-150C sample with a density of 8.21 Ti atoms/nm<sup>2</sup> has a higher edge energy of 3.78 eV compared with that of the 4TS-150C sample, which only contains 5.19 Ti atoms/nm<sup>2</sup>. The changes in observed edge energies are due not only to differences in the deposition rate but also to changes in the precursor-related growth mechanism.

**4.2. Acidity of Supported Titania ALD Films.** The acidity of TiO<sub>2</sub>/SiO<sub>2</sub>-mixed oxides and TiO<sub>2</sub>/SiO<sub>2</sub>-supported oxides has been controversial since Tanabe's proposal that new Brønsted acid sites could be created by a charge imbalance at Ti–O–Si interfaces in the SiO<sub>2</sub>-rich range.<sup>15</sup> The acidity of uniform TiO<sub>2</sub>/SiO<sub>2</sub>-supported oxides prepared by ALD has been investigated by DRIFTS and Raman spectroscopy in the current study.

Pyridine, a commonly used basic probe molecule, was employed to study acid sites on the surface. The surface OH stretch region and the 8a, 8b, 19a, and 19b vibrational bands (following Wilson's numbering)<sup>53</sup> of adsorbed pyridine (point group C<sub>2v</sub>, vibrational modes are derived from that of the parent molecule benzene<sup>42,43,50</sup>) were examined. The 8b and 19b modes are most commonly used in IR studies to evaluate the strength of Lewis acid sites, while the 8a and 19a modes have been used to detect Brønsted acid sites.<sup>18,42,43,50</sup> As shown in Figures 3–5, all of the as-prepared TiO<sub>2</sub>/SiO<sub>2</sub> samples from TiCl<sub>4</sub> showed two pronounced peaks at 1538 (19a mode) and 1637 cm<sup>-1</sup> (8a mode) and an OH stretch mode red shifted by ~1200 cm<sup>-1</sup>, indicative of Brønsted acid sites on these samples. The samples

without chlorine impurities did not show these two pyridinium ion peaks, and the OH stretch mode also exhibited a smaller red shift of  $\sim 1020\text{ cm}^{-1}$ , close to the red shift for pyridine on the pure silica powders ( $965\text{ cm}^{-1}$ ). Therefore, the Brønsted acid sites observed in the DRIFT spectra must be related to chlorine impurities. This conclusion is further confirmed by pyridine adsorption on the calcined 4TS-TTIP-150C (Figure 4g) and 10TS-TTIP-150C samples (Figure 5d).

Raman spectroscopy using pyridine as a probe molecule has also been applied to study the acidity of oxides, although it is less common than the IR technique. Previous work has mainly focused on the two ring-breathing modes  $\nu_1$  and  $\nu_{12}$  near  $1000\text{ cm}^{-1}$  and the  $\nu_2$  CH stretch mode near  $3000\text{ cm}^{-1}$  because they have the strongest intensity.<sup>46,47,49</sup> Hendra et al.<sup>46</sup> pointed out that the Raman shift regions of the  $\nu_1$ ,  $\nu_{12}$ , and  $\nu_2$  vibrational modes are  $996\text{--}1005$ ,  $1032\text{--}1040$ , and  $3064\text{--}3072\text{ cm}^{-1}$  for HPy;  $1007\text{--}1015$ ,  $1025\text{--}1035$ , and  $3090\text{--}3105\text{ cm}^{-1}$  for BPy; and  $1018\text{--}1028$ ,  $1040\text{--}1050$ , and  $3072\text{--}3087\text{ cm}^{-1}$  for Lewis-coordinated pyridine (LPy). The frequency shift of  $\nu_1$ , the totally symmetric ring-breathing mode, away from  $991\text{ cm}^{-1}$  has been correlated with the strength of Lewis acid sites. These three vibrational modes have been used to detect BPy, but the bands are strongly overlapping with HPy and LPy, complicating the study of Brønsted acid sites on the surface using Raman spectroscopy. Little attention has been paid to other vibrational modes such as  $\nu_{6b}$  and  $\nu_{9a}$ , two in-plane C–H bending modes, for the study of acidity, especially Brønsted acid sites.<sup>47</sup>

Solution phase Raman spectra of pyridine (Figure 7) exhibit bands throughout the  $500\text{--}3200\text{ cm}^{-1}$  range. The most intense vibrational modes are  $\nu_1$ ,  $\nu_{12}$ , and  $\nu_2$ . The  $\nu_1$  and  $\nu_{12}$  band positions of HPy ( $1003$  and  $1034\text{ cm}^{-1}$ ) and BPy ( $1010$  and  $1028\text{ cm}^{-1}$ ) are rather close, demonstrating the difficulty of distinguishing these species in adsorbed pyridine. In the case of TiO<sub>2</sub>, pyridine bound to weak Lewis acid sites has been reported to give a  $\nu_1$  band at  $1016\text{ cm}^{-1}$ ,<sup>46</sup> further complicating the separation of HPy, LPy, and BPy. However,  $\nu_{6b}$  and  $\nu_{9a}$ , two in-plane C–H bending modes, have much less overlap between BPy and HPy and provide an additional possibility to distinguish Brønsted acid sites on the surface using Raman spectroscopy. Indeed, two distinct peaks at  $638$  and  $1200\text{ cm}^{-1}$ , observed on the as-prepared 4-cycle samples prepared with TiCl<sub>4</sub> (Figure 6a,b), can be assigned to BPy by comparison with the Raman spectrum of pyridine in HCl solution (Figure 7d), which is in agreement with DRIFTS measurements. Both spectroscopic measurements provide strong evidence that Brønsted acid sites present on the as-prepared TiO<sub>2</sub>/SiO<sub>2</sub> samples are caused by chlorine or carbonyl impurities rather than by the intrinsic Ti–O–Si interface.

The TiO<sub>2</sub>/SiO<sub>2</sub>-supported oxides without chlorine or carbonyl groups did not show any Brønsted acid sites, even though 4-cycle and 10-cycle samples contain mainly 5-fold and 6-fold coordinated Ti cations, as indicated by UV–vis DRS. The results from the present work therefore support Notari's conclusions. However, it should be noted that the absence of Brønsted acid sites on TiO<sub>2</sub>/SiO<sub>2</sub>-supported oxides may be associated with the coordination number of oxygen anions that are bonded to interfacial Ti cations. According to Tanabe's hypothesis, when the oxygen anions bonded to Ti cations are 2-coordinate, i.e., maintain the coordination number of SiO<sub>2</sub>, then Brønsted acid sites should be formed. If the oxygen bonded to Ti is 3-coordinate, the charge imbalance at the interface would be significantly reduced, and Brønsted acid sites would not be formed.<sup>15</sup> Whether it is possible to manipulate the oxygen

coordination number by annealing or using alternative sources of silica remains to be determined.

## 5. Conclusions

ICP measurements show that the deposition rate of titania films on silica gel from TiCl<sub>4</sub> is stable in the  $150\text{--}300\text{ }^\circ\text{C}$  temperature range at approximately  $1.1\text{--}1.0$  Ti atoms/nm<sup>2</sup> per cycle. The deposition rate from TTIP at  $150\text{ }^\circ\text{C}$  is slightly lower, with a value of  $0.8$  Ti atoms/nm<sup>2</sup> per cycle. UV–vis DRS shows that the coordination geometry of Ti cations depends on the number of TiCl<sub>4</sub> ALD cycles and is essentially independent of deposition temperature. Comparatively larger differences in the structures of titania films are observed between those from two different precursors. This is due not only to the difference in deposition rate but also to changes in the precursor-related growth mechanism.

All of the TiO<sub>2</sub>/SiO<sub>2</sub> ALD samples studied exhibit Lewis acidity, but only those containing either chloride or carbonyl impurities possess Brønsted acid sites. In the Raman spectra of as-prepared samples from TiCl<sub>4</sub>, three new pronounced features at  $638$ ,  $1200$ , and  $3103\text{ cm}^{-1}$  were assigned to pyridinium ions. These results provide strong evidence that these three bands,  $\nu_{6b}$  ( $638\text{ cm}^{-1}$ ),  $\nu_{9a}$  ( $1200\text{ cm}^{-1}$ ), and  $\nu_2$  ( $3103\text{ cm}^{-1}$ ), provide an additional spectroscopic signature for Brønsted acid sites on the surface.

**Acknowledgment.** This work was financially supported by the Office of Basic Energy Sciences, U.S. Department of Energy (Grant DE-FG02-97ER14789). The ALD system construction was funded by the Air Force Office of Scientific Research (AFOSR) (MURI F49620-02-1-0381 and DURIP FA-9550-07-1-0526) and the Defense Threat Reduction Agency (DTRA) JSTO FA9550-06-1-0558. The authors thank Jeffrey W. Elam and Joseph A. Libera for technical assistance.

## References and Notes

- Gao, X.; Wachs, I. E. *Catal. Today* **1999**, *51*, 233.
- Itoh, M.; Hattori, H.; Tanabe, K. *J. Catal.* **1974**, *35*, 225.
- Khouw, C. B.; Dartt, C. B.; Labinger, J. A.; Davis, M. E. *J. Catal.* **1994**, *149*, 195.
- Liu, Z.; Tabora, J.; Davis, R. J. *J. Catal.* **1994**, *149*, 117.
- Sohn, J. R.; Jang, J. H. *J. Catal.* **1991**, *132*, 563.
- Srinivasan, S.; Datye, A. K.; Hampden-Smith, M.; Wachs, I. E.; Deo, G.; Jehng, J. M.; Turek, A. M.; Peden, C. H. F. *J. Catal.* **1991**, *131*, 260.
- Srinivasan, S.; Datye, A. K.; Smith, M. H.; Peden, C. H. F. *J. Catal.* **1994**, *145*, 565.
- Klein, S.; Martens, J. A.; Parton, R.; Vercautse, K.; Jacobs, P.; Maier, W. F. *Catal. Lett.* **1996**, *38*, 209.
- Castillo, R.; Koch, B.; Ruiz, P.; Delmon, B. *J. Catal.* **1996**, *161*, 524.
- Elguezabal, A. A.; Corberan, V. C. *Catal. Today* **1996**, *32*, 265.
- Dias, C. R.; Portela, M. F.; Galan-Fereres, M.; Banares, M. A.; Granados, M. L.; Pena, M. A.; Fierro, J. L. G. *Catal. Lett.* **1997**, *43*, 117.
- Gao, X.; Bare, S. R.; Fierro, J. L. G.; Banares, M. A.; Wachs, I. E. *J. Phys. Chem. B* **1998**, *102*, 5653.
- Bonelli, B.; Cozzolino, M.; Tesser, R.; Di Serio, M.; Piumetti, M.; Garrone, E.; Santacesaria, E. *J. Catal.* **2007**, *246*, 293.
- Notari, B.; Willey, R. J.; Panizza, M.; Busca, G. *Catal. Today* **2006**, *116*, 99.
- Tanabe, K.; Sumiyoshi, T.; Shibata, K.; Kiyoura, T.; Kitagawa, J. *Bull. Chem. Soc. Jpn.* **1974**, *47*, 1064.
- Ko, E. I.; Chen, J. P.; Weissman, J. G. *J. Catal.* **1987**, *105*, 511.
- Liu, Z.; Tabora, J.; Davis, R. J. *J. Catal.* **1994**, *149*, 117.
- Doolin, P. K.; Alerasool, S.; Zaleski, D. J.; Hoffman, J. F. *Catal. Lett.* **1994**, *25*, 209.
- Guo, D.-S.; Ma, Z.-F.; Yin, C.-S.; Jiang, Q.-Z. *Chin. J. Chem. Phys.* **2008**, *21*, 21.
- Suntola, T.; Antson, J. Method for Producing Compound Thin Films. U.S. Patent 4058430, 1977.
- Ritala, M. *Appl. Surf. Sci.* **1997**, *112*, 223.

- (22) Chen, R.; Kim, H.; McIntyre, P. C.; Bent, S. F. *Appl. Phys. Lett.* **2004**, *84*, 4017.
- (23) Mayer, T. M.; Elam, J. W.; George, S. M.; Kotula, P. G. *Appl. Phys. Lett.* **2003**, *82*, 2883.
- (24) Keränen, J.; Carniti, P.; Gervasini, A.; Iiskola, E.; Auroux, A.; Niinistö, L. *Catal. Today* **2004**, *91*, 67.
- (25) King, J. S.; Wittstock, A.; Biener, J.; Kucheyev, S. O.; Wang, Y. M.; Baumann, T. F.; Giri, S. K.; Hamza, A. V.; Baeumer, M.; Bent, S. F. *Nano Lett.* **2008**, *8*, 2405.
- (26) Herrera, J. E.; Kwak, J. H.; Hu, J. Z.; Wang, Y.; Peden, C. H. F. *Top. Catal.* **2006**, *39*, 245.
- (27) Haukka, S.; Lakomaa, E. L.; Suntola, T. *Stud. Surf. Sci. Catal.* **1998**, *120*, 715.
- (28) Stair, P. C. *J. Chem. Phys.* **2008**, *128*, 182507.
- (29) Ritala, M.; Leskelii, M.; Niinistö, L.; Haussalo, P. *Chem. Mater.* **1993**, *5*, 1174.
- (30) Ritala, M.; Leskelii, M.; Nykänen, E.; Soininen, P.; Niinistö, L. *Thin Solid Films* **1993**, *225*, 295.
- (31) Aarik, J.; Aidla, A.; Uustare, T.; Sammelselg, V. *J. Cryst. Growth* **1995**, *148*, 268.
- (32) Aarik, J.; Aidla, A.; Mändar, H.; Uustare, T. *Appl. Surf. Sci.* **2001**, *172*, 148.
- (33) Gu, W.; Tripp, C. P. *Langmuir* **2005**, *21*, 211.
- (34) Lakomaa, E.-L.; Haukka, S.; Suntola, T. *Appl. Surf. Sci.* **1992**, *60–61*, 742.
- (35) Ferguson, J. D.; Yoder, A. R.; Weimer, A. W.; George, S. M. *Appl. Surf. Sci.* **2004**, *226*, 393.
- (36) Keränen, J.; Iiskola, E.; Guimon, C.; Auroux, A.; Niinistö, L. *Stud. Surf. Sci. Catal.* **2002**, *143*, 777.
- (37) Elam, J. W.; Groner, M. D.; George, S. M. *Rev. Sci. Instrum.* **2002**, *73*, 2981.
- (38) Libera, J. A.; Elam, J. W.; Pellin, M. J. *Thin Solid Films* **2007**, *516*, 6158.
- (39) Barrett, E. P.; Joyner, L. G.; Halenda, P. P. *J. Am. Chem. Soc.* **1951**, *73*, 373.
- (40) Chua, Y. T.; Stair, P. C. *J. Catal.* **2000**, *196*, 66.
- (41) Arena, F.; Frusteri, F.; Mondello, N.; Giordano, N.; Parmaliana, A. *J. Chem. Soc., Faraday Trans.* **1992**, *88*, 3353.
- (42) Busca, G. *Catal. Today* **1998**, *41*, 191.
- (43) Busca, G. *Phys. Chem. Chem. Phys.* **1999**, *1*, 723.
- (44) Castillo, R.; Koch, B.; Ruiz, P.; Delmon, B. *J. Catal.* **1996**, *161*, 524.
- (45) Hendra, P. J.; Horder, J. R.; Loader, E. J. *Chem. Commun.* **1970**, 563.
- (46) Hendra, P. J.; Turner, I. D. M.; Loader, E. J.; Stacey, M. *J. Phys. Chem.* **1974**, *78*, 300.
- (47) Heaviside, J.; Hendra, P. J.; Paul, S. O.; Freeman, J. J.; Friedman, R. M. *Appl. Spectrosc.* **1981**, *35*, 220.
- (48) Matzner, R. A.; Bales, R. C.; Pemberton, J. E. *Appl. Spectrosc.* **1994**, *48*, 1043.
- (49) Yamada, H.; Yamamoto, Y. *J. Chem. Soc., Faraday Trans. 1* **1979**, *75*, 1215.
- (50) Dollish, F. R.; Fateley, W. G.; Bentley, F. F. *Characteristic Raman Frequencies of Organic Compounds*; Wiley: New York, 1974; Vol. 18, pp 263–266.
- (51) Klein, S.; Weckhuysen, B. M.; Martens, J. A.; Maier, W. F.; Jacobs, P. A. *J. Catal.* **1996**, *163*, 489.
- (52) Schrijnemakers, K.; Impens, N. R. E. N.; Vansant, E. F. *Langmuir* **1999**, *15*, 5807.
- (53) Wilson, E. B., Jr. *Phys. Rev.* **1934**, *45*, 706.

JP902200C